Journal of King Saud University – Science 32 (2020) 3351–3358

Contents lists available at ScienceDirect

Journal of King Saud University – Science

journal homepage: www.sciencedirect.com

Original article

Self-nitrogen doped carbons aerogel derived from waste cigarette butts (cellulose acetate) for the adsorption of BPA: Kinetics and adsorption mechanisms

Norah S. Alhokbany [a], Mu Naushad [a,b], Vikrant Kumar [c], Saad Al hatim [a], Saad M. Alshehri [a], Tansir Ahamad [a,*]

[a] Department of Chemistry, College of Science, King Saud University, Riyadh, Saudi Arabia
[b] School of Life and Allied Health Sciences, Glocal University, Saharanpur, India
[c] Research Laboratory of Inorganic Chemistry, Department of Chemistry, Acharya Narendra Dev College, (University of Delhi), Govindpuri, Kalka Ji, New Delhi 110019, India

ARTICLE INFO

Article history:
Received 21 May 2020
Revised 10 September 2020
Accepted 12 September 2020
Available online 25 September 2020

Keywords:
Cellulose acetate
Nicotine
Nanocomposite
FTIR
Bisphenol-A
N-doped carbon

ABSTRACT

The fabrication of highly porous functionalized carbon materials is the demand of current scenario for the removal of toxic pollutants form aqueous solution. Therefore, waste cigarette butts that consist of cellulose acetate and other nitrogen rich compounds, such as nicotine and harmine have been used for the fabrication of N-doped carbon aerogel (NDC) via hydrothermal and carbonization process. As-fabricated NDC was characterized via, elemental analysis, FTIR, Raman, TGA, XRD, BET, SEM and XPS and used for the adsorption of bisphenol –A (BPA). The outcomes of adsorption essay and its kinetics support that the adsorption of BPA over NDC was carried out via pseudo-second-order kinetic model and via Langmuir model isotherm. The values for ΔG and ΔH were found negative and positive respectively, and support that the adsorption process is spontaneous and endothermic. The nature of adsorbent as well as in-situ and post characterization of the adsorbent support the adsorption mechanism, and the conclusions support that the hydrogen bonding, electrostatic as well as the π-π interactions were employed between the BPA and NDC during adsorption. In addition, the regeneration of the NDC was efficiently achieved and BPA removal efficiency remained high (92.47%) after seven cycles.

1. Introduction

Water pollution has always been a serious worldwide problem and it has concerned the attention of researchers all over the world. Several industries including fabric, printing and tissue, paints, plastics and leather, etc. use different type of organic dyes, heavy metals and organic phenols and expose to the environment. Among these pollutants, bisphenol-A (BPA), which is used for the manufacture of several polymers and plastics and noticed as an endocrine disruptor compounds (EDCs) has several health issue including cancer, hormonal imbalance, abnormal reproductive and developmental behavior (Sophia and Lima, 2018; Wang et al., 2019a, 2019b). Due to these health issues, it is essential to eliminate BPA from wastewaters, prior to discharge into the environment. Several methods such as biodegradation, filtration, fenton chemical oxidation, photocatalytic degradation and adsorption have been employed for the management of BPA in contaminated water and other pollutants with variable success (Shokry et al., 2019; Soliman et al., 2019; Zhang et al., 2019). Among these methods, adsorption stands as one of the best available techniques due to its easy operation, cost-effective, feasibility, time and energy saving (Xiaoying et al., 2009). Hence, many adsorbents, such as metal oxides, graphite carbon/CNTs, bio-adsorbents, clay and polymers have been used for the adsorption of BPA from waste water. Among these adsorbent, carbon based adsorbents such as carbon nanotubes, activated carbon, and graphene have been extensively used for the removal pollutants form aqueous solution due to their high surface area and due to their excellent mechanical properties. Although, these pure carbonaceous materials are very stable but have two drawbacks, firstly the high costs and regeneration and secondly, poor adsorption capacity due to

* Corresponding author.
E-mail address: tahamed@ksu.edu.sa (T. Ahamad).
Peer review under responsibility of King Saud University.

Production and hosting by Elsevier

https://doi.org/10.1016/j.jksus.2020.09.021
1018-3647/

the lack of active sites or heteroatoms (Liu et al., 2016). Therefore, the fabrication of highly porous functionalized carbon materials is the demand of current scenario for the removal of toxic pollutants form aqueous solution. Previously several highly porous carbon nanocomposites have been prepared using municipal waste materials or agriculture waste (Choi and Kan, 2019; Liu et al., 2020; Rong et al., 2019). Between these municipal waste materials is our main interest, specially cigarette butts (Kurmus and Mohajerani, 2020). It was recorded that about to 5.8 trillion cigarette butts are thrown to the environment annually, resulting 8×10^5 metric ton municipality waste. The cigarette butts are prepared using natural polymer (cellulose acetate). Cellulose acetate is potential source to fabricate highly porous carbon than coal-based carbonaceous precursors. The utilization of the municipal waste cigarette butts for the fabrication of highly porous carbon, that not only solve the municipality and environmental issue but also provide the new source of the carbon materials (Yu et al., 2018). Keeping these evidences, In the present study we have select waste cigarette butts that consist of cellulose acetate and other nitrogen rich compounds (nicotine and harmine) as a single source precursor for the fabrication of nitrogen self-doped activated carbons via a hydrothermal and carbonization process.

2. Experimental

The waste cigarette butts were collect locally in the smoking zone, and crushed in a mechanical grinder. 4.0 g of used cigarette butts powder was sonicated with 30 ml of distilled water for 30 min and then transferred into an autoclave (200 ml) with a teflon liner followed by hydrothermal treating at 180 °C for 24 h to get hydrated biochar. After cooling the autoclave, the obtained biochar was washed with dil 0.1 M HCl and then with distilled water and dried off in vacuum oven overnight then pyrolysed at 800 °C with a heating rate 5 °C/min under the flow of Ar. (Ahamad et al., 2019c; Al-Kahtani et al., 2019; Naushad et al., 2017). The details of analytical techniques and batch adsorption assay are given in supporting information.

3. Results and discussion

3.1. Characterization of NDC

The synthesis of the NDC is schematically illustrated in Fig. 1, the elemental analysis of the NDC show the presence of C (82.41%) and N (14.89%) support the presence of N- heteroatom in NDC while in the case of biochar the elemental results were found to be C (64.42%), N (4.34%) and O (30.54%). The FTIR spectra

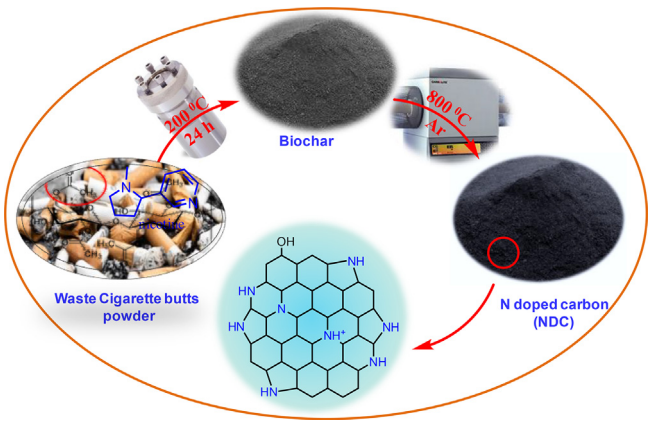

Fig. 1. The synthesis routes for the synthesis of NDC.

of the waste cigarette butts (WCB) powder, biochar and NDC are illustrated in Fig. 2(a), the results exposed that the WCB and the biochar have several organic functional groups and show the FTIR peaks at 3400–3202, 3050, 2941–2843, 1613, 1506, 1447, 1345, 1124 cm^{-1} and assigned to OH-NH, C═CH, —CH, —COOH, C═O, C═C, C—N/C—O, C—H functional groups respectively (Ahamad and Nishat, 2008; Nishat et al., 2011). While in the case of NDC some peaks are disappear or become fewer instances due to the rearrangement of the functional groups during hydrothermal and thermal treatment of the compounds. The FTIR spectra of the NDC show peaks at 3420 and 3345 cm^{-1} and assigned to O—H/N—H stretching vibrations. The sharp absorption peaks at 1659 and 1566 cm^{-1} are due to the presence of C═O and C═C functional groups, respectively (Ahamad and Alshehri, 2014). Other peaks at 1172, 1360 and 1483 cm^{-1} are assigned to C—O, C—N and C═C respectively (Alshehri et al., 2016).

The TGA of the biochar and the NDC shown in Fig. 2(b), the TGA plot of the biochar shows four stage of thermal degradation. The first stage between room temperature and 170 °C, in this region 21.21% weight loss was found (Al-Farraj et al., 2018). The second and third degradation is the main degradation step and in these step 28.21 and 24.15% loss were notices. The last stage is the cracking of the materials and it is slow degradation between 450 and 1000 and 20.21% weight of the total weight was degraded. However, with NDC, only two slow degradations were found and initially 5.70% weight loose was notices up to 170 °C. In the second degradation stage 8.42% weight loss was observed between 150 and 350 °C. The residue weight at 1000 °C, were found to be 28.99% and 74.21% for biochar and NDC respectively (Ahamad and Alshehri, 2013; Alshehri and Ahamad, 2013; Alshehri et al., 2013). The NDC show superior thermal stability than that of the biochar because the NDC is pre –heat treated under the flow of Ar. The XRD spectra of the NDC is shown in Fig. 2(c), the XRD spectra of the biochar show amorphous nature and no sharp peaks was observed while the XRD spectra of the NDC showed two peaks at 2θ of 23.72° and 43.18°, assigned to (0 0 2) and (0 0 4) planes of graphite carbon (Wen et al., 2019; Xiao et al., 2019). Raman spectra of NDC is shown Fig. 2(d), the Raman spectra show two bands at 1322.7 cm^{-1} and 1587.6 cm^{-1}assigned to the disordered sp^3carbons (D-band) and the latter by graphitic sp^2carbons (G-band). (Alhokbany et al., 2019; Guo et al., 2011). The I_D/I_G value was found to be 1.22, that support the presence of disordered carbon. The doping of the nitrogen in the activated carbon aerogel opens new channels for the adsorption of BPA. N_2 adsorption/desorption isotherms exhibited that the fabricated NDC possessed Type IV isotherms with hysteresis loops and support the presence of mesoporous structure. The BET specific surface area of NDC is found to be 841 m^2/g and the N2 adsorption desorption plots are shown in supporting figure SF1 (a). The pore width distribution as shown in supporting figure SF1 (b), show the presence of hierarchical pore structures with pore volumes (from 0.19 to 1.28 cm^3 /g) for NDC. It is envisaged that the mesoporous structure of NDC will allow the BPA to the active sites with minor diffusion limitations. The morphology of the fabricated carbon was determine using SEM image as shown in Fig. 3(a-b), The SEM image of the NDC show porous structures composed of small particles. Further the morphology was determined with TEM as shown in Fig. 3(c). The images support the presence of porous structure of the NDC with ultrafine structure. On the whole, all the results (FTIR, XRD, Raman, SEM, and TEM) above demonstrate that the used cellulose acetate powder have been used as a self-doping agent for the fabrication of nitrogen doped carbon by efficient hydrothermal synthesis method.

The XPS survey of samples is shown in Fig. 4(a), the spectra display the presence of C, N and O elements and the peaks occurs at 284.8 eV, 399.7 and 531.2 eV respectively. Fig. 4(b), the C1s spectra

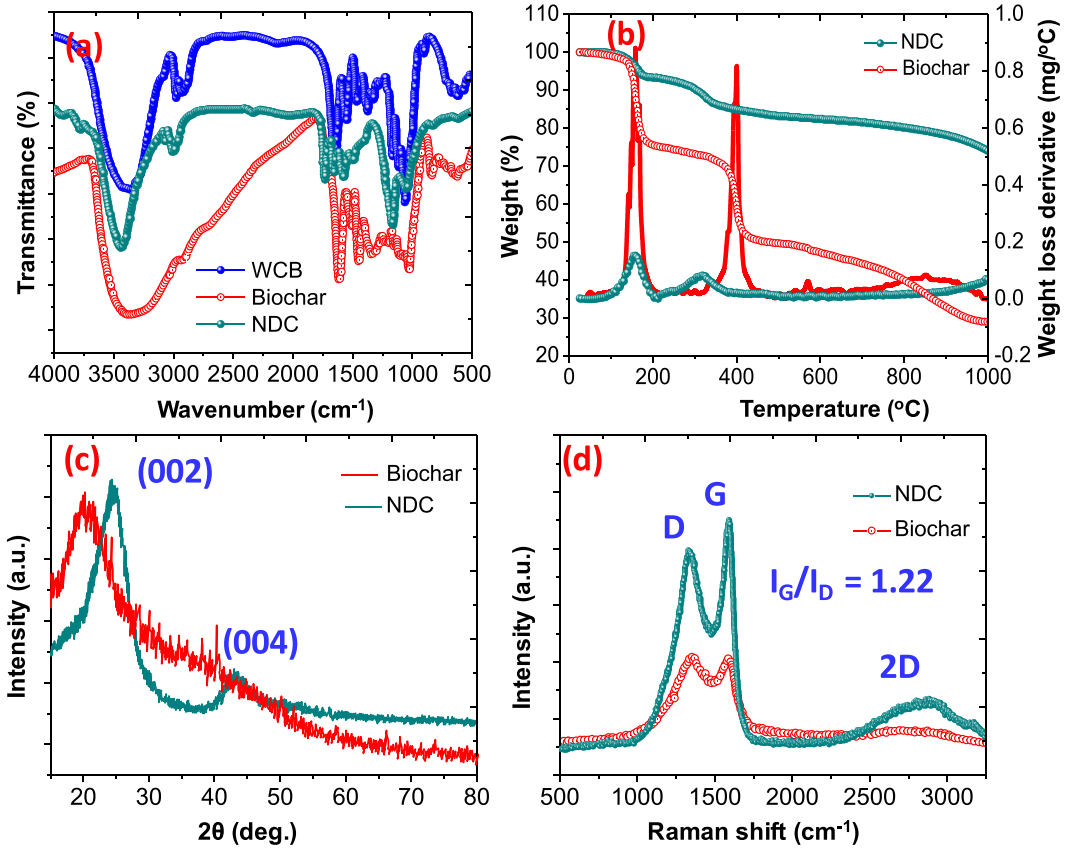

Fig. 2. (a) FTIR spectra of WCB, biochar, and NDC (b) TGA/DTA curves of biochar, and NDC (c) XRD of biochar, and NDC (d) Raman spectrum for biochar, and NDC.

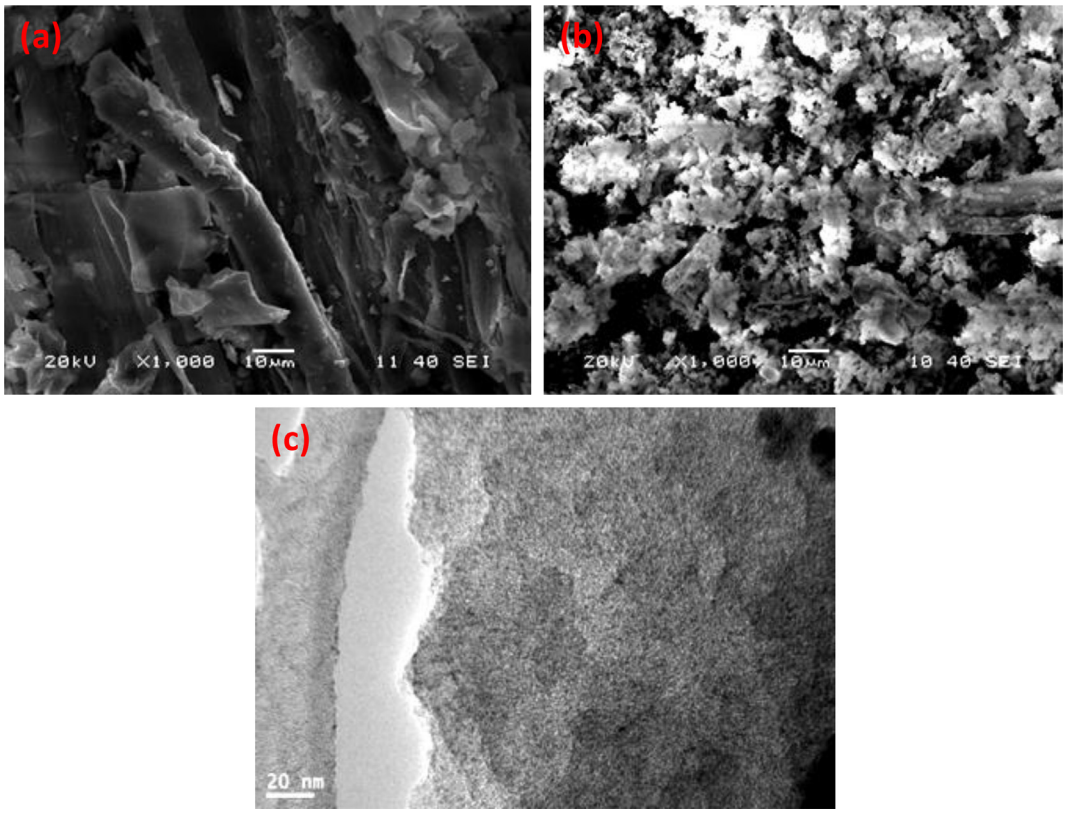

Fig. 3. (a) SEM image of biochar (b) SEM image of NDC (c) TEM image of NDC.

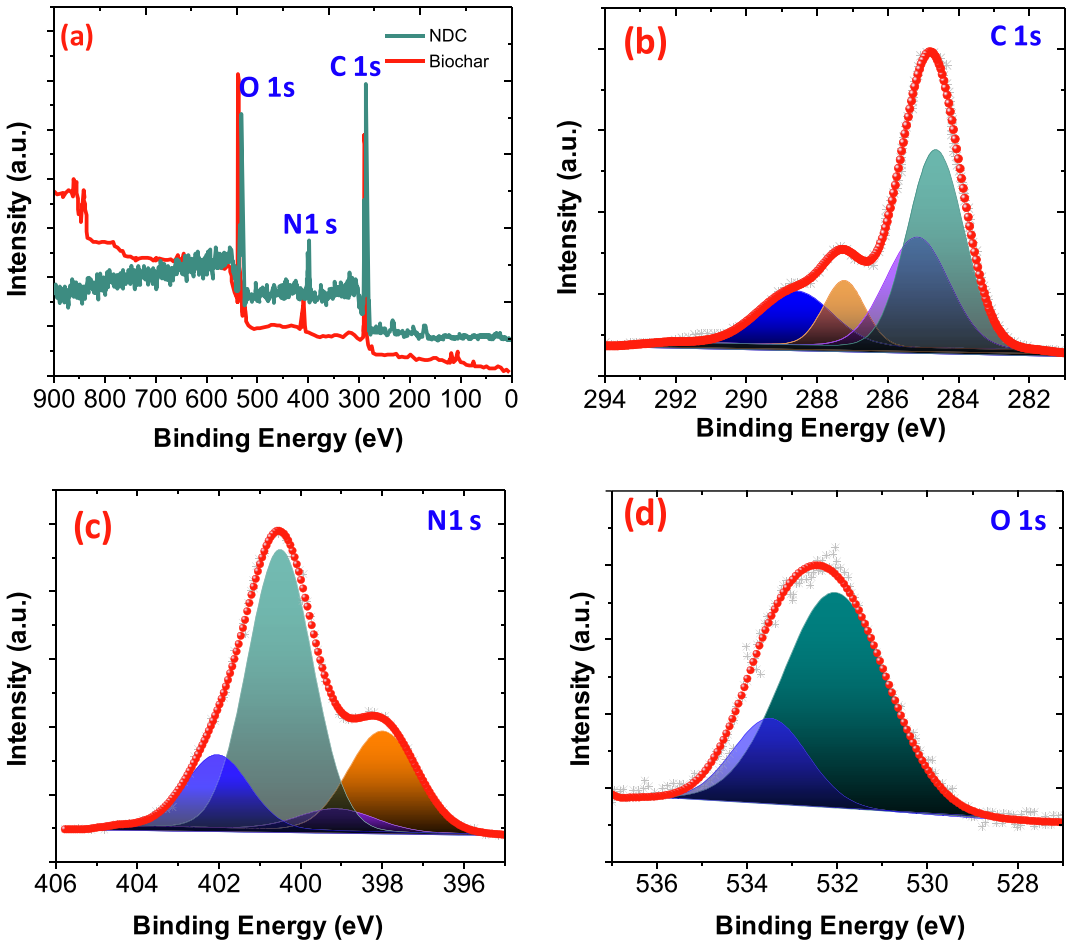

Fig. 4. (a) A wide XPS spectra for biochar and NDC (b) C 1s, (c) N 1sand (d) O 1s,

can be split into four different peaks, the main peak at 284.47 eV (C = C) related to graphitic sp^2 C atoms, involving successful carbonization of biochar composite and occupied about the highest peak area. In addition, two more peaks appeared at 285.36 and 286.85 eV could be attributed to C-N and C-OH and support successful incorporation of N and O atoms and formation of new sites in to the NDC based adsorbent(Al-Kahtani et al., 2018; Alshehri et al., 2018). High-resolution N1s spectra split into four types of nitrogen species at 397.90 eV, 398.81 eV, 400.51 eV and 402.04 assigned to pyridinic-N, pyrrolic-N, quaternary-N and N-Ox, respectively as illustrated in Fig. 4(c) (Al-Enizi et al., 2018). The O1s show peaks related to C—O, and C=O which appeared at 532.43 eV and 533.0 eV respectively as shown in Fig. 4(d). To verify the hydrophobic and hydrophilic behavior of the biochar and the NDC, the contact angles were measured. It was noticed, when a water drop was placed on the biochar, the water was completely speared onto the surface, resulting no contact angle was observed. However, after the pyrolysis of bio-char, the hydrophilic nature of the NDC was changed. When, a drop of water was deposited on the surface of NDC, the value of contact angle of the water droplet was 132°.

3.2. Batch adsorption studies

Batch adsorption experiments were performed between pH 3–13, initial concentration (5–200 mgL^{-1}), dose of the adsorbent (0.05–1.0 g) and wide range of contact time (0–180 min). During the adsorption experiments only one factor was changed and other factors remains constant to estimate the optimal values of the adsorption factors. At room temperature the optimal pH, initial concentration, does of adsorbent and contraction time for the adsorption of BPA over NDC were found to be pH 7, 60 mgL^{-1}, 0.2 g, and 60 min respectively.

3.2.1. Effect of pH and dose

The effect of initial pH plays an important role during the adsorption of BPA over NDC, when the pH was increased form 3–12 the adsorption capacity of the NDC was varied. As shown in Fig. 5(a). It was notices when the pH was raised from 2 to 9 the adsorption capacity of the adsorbent was increased rapidly up to pH 7 and then become slow up to 9. However, when the initial pH was raised from 9 to 12 the adsorption of BPA was decreased. This is because in higher pH the BPA changed into electron rich ions bisphenolate because of pH > pKa, (pKa for BPA 9.6–10.2). As we know that the NDC have free electrons and negatively charged surface and behave as a Lewis base. Therefore, at higher pH an electrostatic repulsion was occurs and resulting the significant change was noticed. When the pH was less than pKa no electrostatic repulsion was notices, the maximum adsorption is observed at pH 9 (318.4 mg/g), this adsorption capacity is little much higher form the pH 7 (310.5). Therefore, the optimal pH 7 was used in this study.

3.2.2. Effect of initial concentration

At optimal condition, the initial concentration of BPA was change from 5 mg/L to 200 mg/L, resulting the significant change

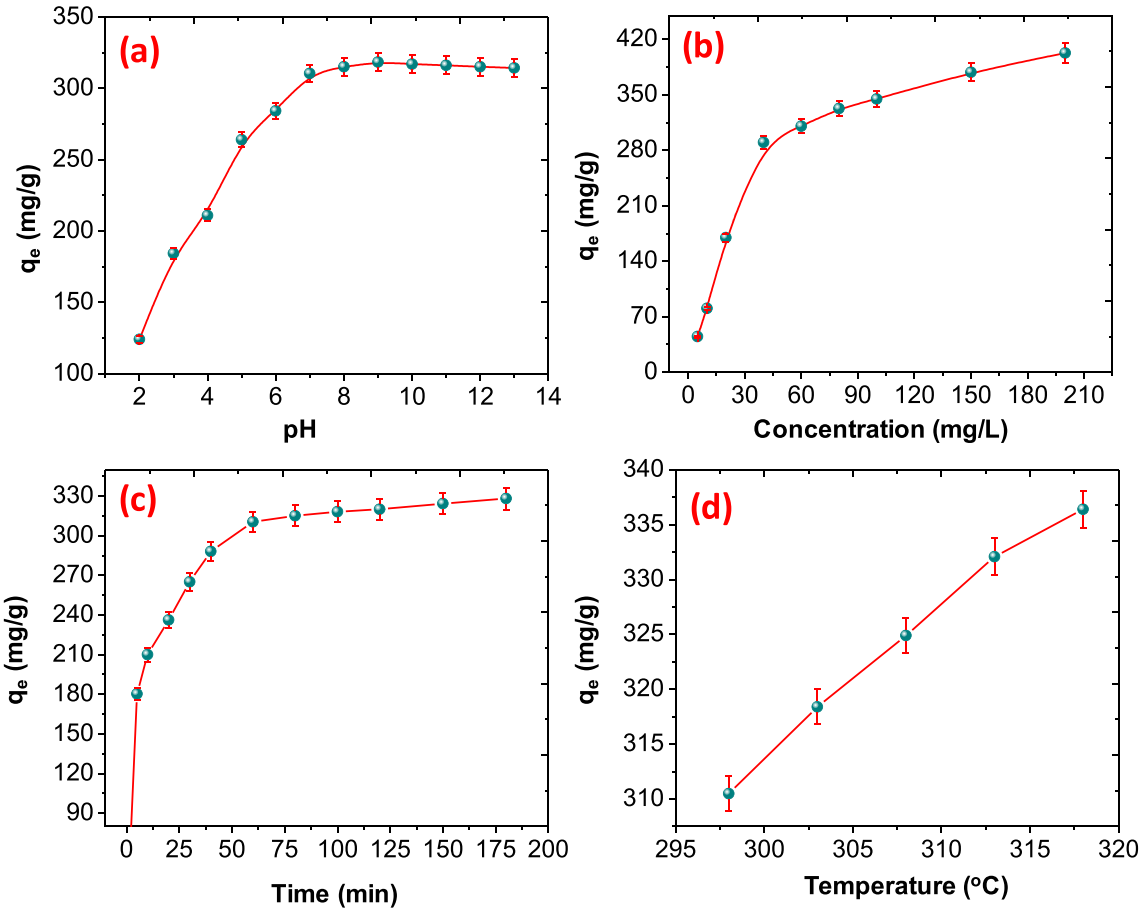

Fig. 5. Effect of (a) pH (b) concentration (c) time and (d) temperature on the adsorption of BPA onto NDC.

was noticed. As shown in Fig. 5(b), As the concentration of BPA was raised from 5 to 60 mg/L, the adsorption capacity of the NDC was increased rapidly and found to be 310.5 mg/g. moreover, when the concentration was further increased up to 100 mg/L, the adsorption capacity increased slowly and found to be 344.62 mg/g, then become saturated at 200 mg/L and found to be 402.67 mg/g. this is because when the initial concentration of the adsorbate was increased the active sites on the adsorption was decreased and the adsorption process was decreased (Ahamad et al., 2019a, 2019b).

3.2.3. Effect of contact time

The effect of contact time during the adsorption of BPA over NDC was studied. As shown in Fig. 5(c), at the optimal adsorption condition, the adsorption capacity of the NDC was increased gradually in early stage and found to be 310.5 mg/g after 60 min. When the adsorption time was increased from 60 to150 min the adsorption capacity is observed 324.44 mg/g. while the rate of adsorption become slow and then saturate at 180 min and found to be 328.18 mg/g. This is because in initial the adsorption occurs fast due to the availability of adsorption sites and later become slow due to insufficient adsorption site on the surface of the NDC, resulting adsorption increased gradually. On the other hand at higher concentration and late adsorption stage, the insufficient contact between BPA and the NDC in the late stage and eventually full occupation of active adsorption sites on the NDC (Ahamad et al., 2019d, 2019e).

3.2.4. Adsorption kinetics and adsorption isotherm

To determine the adsorption kinetics for the adsorption of BPA onto NDC, pseudo-first-order, pseudo-second-order and intra-particle diffusion kinetic models have been used and the details of the models and their relative parameters are explained in Supporting Information. The experimental data were fitted and illustrated in Fig. 6(a) and the results are summarized in Table 1. According to the parameter values and R^2 values of these models, the pseudo-second-order kinetic model could effectively describe the adsorption process of BPA and found to be 0.9934. Meanwhile, calculated adsorption capacity of NDC for BPA was found to be 314.21 mg/g by the pseudo-second order model fits the actual experimental results and supports the physio-chemical adsorption of BPA onto NDC via π-π and π-cation interactions and hydrogen bonding.

Adsorption isotherms were used to further explain the adsorption mechanism and the interaction between BPA and NDC. The adsorption isotherm gives details the amount of BPA adsorbed by unit mass of adsorbent at a constant temperature as a function of BPA concentration at equilibration. The isotherm parameters obtained from non-linear fitting of the three different models are illustrated in Fig. 6(b). As can be seen from table-1, although both the Langmuir model provide more satisfactory mathematical fits to the experimental data points (R^2 = 0.9964) than the Freundlich model and Temkin model. The results indicate that the adsorption of BPA on NDC was of a monolayer type. The maximum capacity of NDC for BPA adsorption was 364.21 mg/g.

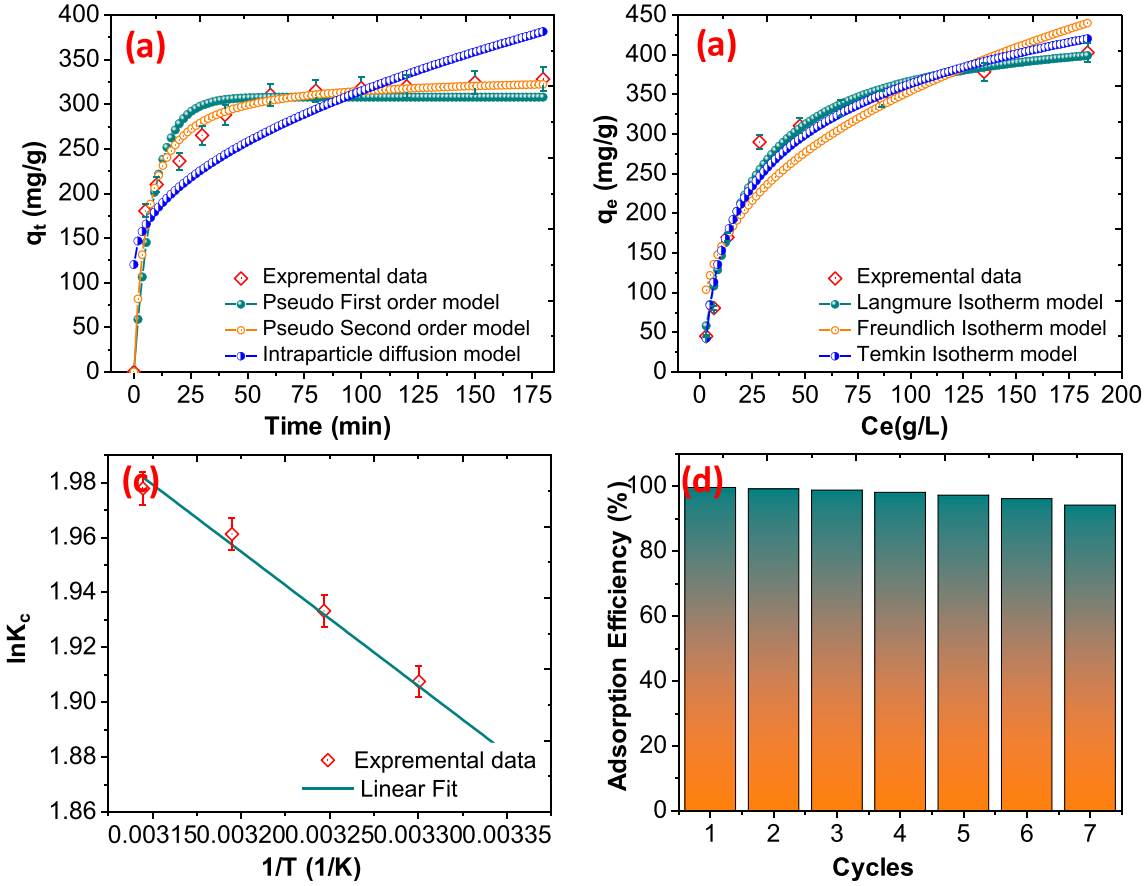

Fig. 6. (a) Adsorption isotherm of BPA on NDC (b) Kinetics of BPA adsorption on NDC (c) adsorption thermodynamic of BPA over NDC (d) regeneration behavior of NDC.

Table 1
Adsorption kinetics and adsorption isotherm parameters for BPA adsorption over NDC

Models	Parameters		
First Order	q_e (mg g^{-1})	k_1(min^{-1})	R ^{2}
	302.02	0.1165	0.9321
Second Order	q_e (mg g^{-1})	k_2 (g mg^{-1} min^{-1})	R ^{2}
	314.21	5.40x10^{-4}	0.9934
Intra-particle diffusion	C	K_{dif} (mg g^{-1} min$^{-1/2}$)	R^2
	120.21	19.45	0.79321
Langmuir isotherm	Q_0 *(mg/g)*	K_L	R^2
	364.21	0.0468	0.9964
Freundlich isotherm	K_F *(mg/g.(L/g)^n)*	n	R^2
	68.34	2.80	0.9014
Temkin isotherm	K_t (L/gm)	Bt	R^2
	0.490	93.28	0.9683

3.2.5. Adsorption thermodynamics

When the temperature of the solution was increased, it affects the adsorption capacity of the NDC and the results are illustrated in Fig. 5(d). It was observed that when the temperature was increased from 298 K to 318 K the adsorption capacity was increased from 310.5 to 336.5 mg/g and supports the endothermic adsorption process. The value of ΔH and ΔS were calculated using the slope and intercept of the Fig. 6(c) and the values were summarized in Table ST 1 (ESI), the ΔG^0 values are negative with all the temperature, which suggests the adsorption process is spontaneous. A positive ΔH° value is evidence of the fact that BPA adsorption on activated carbon aerogel is endothermic and chemisorption. This physio-chemical reaction might be assigned to hydrogen bonding, or Van der waals forces. The positive values of ΔS_0 indicated that the randomness of the system increased during pollutants adsorption.

3.2.6. Regeneration of the adsorbent

The regeneration of the adsorbent is an important factor for their use on industrial scale. In order to explore the reusability of NDC, the BPA was desorbed via aqueous methanol in ultrasonic technique, which can dislodge contaminants attached to the pores in NDC and the adsorption capacity found after each cycles are illustrated in Fig. 6(d). After seven cycles, the NDC show the adsorption capacity about to 94.21%.

3.3. Mechanism of adsorption

The adsorption of the organic pollutants was affected not only via functional groups of the adsorbent but also other factors such as surface properties, porous networks and mass transfer process of NDC in bulk solution. Here, the adsorption of BPA over NDC was proceed via π-π interaction, hydrogen bond, electrostatic interactions and the details of the interaction between the BPA and NDC was determine via FTIR and XPS spectra of the composite after the adsorption and desorption of the BPA as shown in figure SF 2(a) (ESI). When the FTIR spectra of the NDC after BPA adsorption was compared with the pure and regenerated NDC, one peak was shift from 1659 to 1625 cm^{-1}, this is because of the hydrogen bonding (II) between C═O and OH of BPA as shown in figure SF 2(b) (ESI). Another FTIR peak were shifted from 3452 to 3415 (O—H and become broad, additionally the pack belongs to C═O in the case of NDC was shifted from 1754 to 1684 cm^{-1}, this support the presence of hydrogen bonding between the phenolic groups of the BPA and the carbonyl and amino groups of the NDC. The peak at 1460 belongs to NH groups also shifted to the lower frequency and observed at 1452 cm^{-1}, and support the involvement of the

NH or nitrogen doping atoms for the adsorption of BPA over NDC. π-π interaction that was occurs between the aromatic ring of the BPA and the π e^- of the NDC. The XRD spectra of the NDC after the adsorption show in figure SF 2(c) (ESI), the results revealed that there is not significant change in the crystalline nature of the NDC only little change was observed due to the amorphous nature of BPA. The adsorption of the BPA was also further supported via XPS spectra and after the adsorption of the BPA the intensity of C1 s increased due to the adsorption of the BPA as shown in figure SF 2(d) (ESI). On the other hands, some peaks of the C1s spectra is shifted to the other position and support the presence of π-π interaction. While the change in the O1s and N1s also support the presence of hydrogen bonding during the adsorption of BPA (Park et al., 2019).

4. Conclusion

This study introduced the fabrication of self-nitrogen doped carbon aerogel form the waste cigarette butts powder and used for the adsorption BPA from aqueous solution. The fabricated NDC was characterized via several analytical techniques. The batch adsorption of BPA was carried out and the effects of pH value, contact time, temperature and initial concentration were also examined. The results support the presence of pseudo second order kinetics and the Langmuir model provide more satisfactory mathematical fits to the experimental data points (R^2 = 0.9964) than the Freundlich model and Temkin model. The thermodynamic results support that the adsorption process is spontaneous and endothermic. The adsorption mechanism of BPA over NDC was proceed via π-π interaction, hydrogen bond, electrostatic interactions and the details of the interaction between the BPA and NDC was determine via FTIR, XRD and XPS spectra after the adsorption and desorption of the BPA. Finally, regenerated NDC was still effective after 7 regeneration steps, additional prominence the benefits of this useful potential material.

Declaration of Competing Interest

The authors declare that they have no known competing financial interests or personal relationships that could have appeared to influence the work reported in this paper.

Acknowledgement

The authors extend their sincere appreciation to the Deanship of Scientific Research at King Saud University for funding this work through research group no (RG-1438-026).

Appendix A. Supplementary data

Supplementary data to this article can be found online at https://doi.org/10.1016/j.jksus.2020.09.021.

References

Ahamad, T., Alshehri, S.M., 2013. Thermal degradation and evolved gas analysis of epoxy (DGEBA)/novolac resin blends (ENB) during pyrolysis and combustion. J. Therm. Anal. Calorim. 111 (1), 445–451.
Ahamad, T., Alshehri, S.M., 2014. Thermal degradation and evolved gas analysis: A polymeric blend of urea formaldehyde (UF) and epoxy (DGEBA) resin. Arab. J. Chem. 7 (6), 1140–1147.
Ahamad, T., Naushad, M., Eldesoky, G.E., Al-Saeedi, S.I., Nafady, A., Al-Kadhi, N.S., Al-Muhtaseb, A.A.H., Khan, A.A., Khan, A., 2019a. Effective and fast adsorptive removal of toxic cationic dye (MB) from aqueous medium using amino-functionalized magnetic multiwall carbon nanotubes. J. Mol. Liquids 282, 154–161.
Ahamad, T., Naushad, M., Eldesoky, G.E., Alqadami, A.A., Khan, A., 2019b. Synthesis and characterization of egg-albumen-formaldehyde based magnetic polymeric resin (MPR): Highly efficient adsorbent for Cd(II) ion removal from aqueous medium. J. Mol. Liq. 286, 110951.
Ahamad, T., Naushad, M., Ruksana, Alhabarah, A.N., Alshehri, S.M., 2019c. N/S doped highly porous magnetic carbon aerogel derived from sugarcane bagasse cellulose for the removal of bisphenol A. Int. J. Biol. Macromol. 132, 1031–1038.
Ahamad, T., Naushad, M., Ruksana, Alshehri, S.M., 2019d. Ultra-fast spill oil recovery using a mesoporous lignin based nanocomposite prepared from date palm pits (Phoenix dactylifera L.). Int. J. Biol. Macromol. 130, 139–147.
Ahamad, T., Nishat, N., 2008. New antimicrobial epoxy-resin-bearing Schiff-base metal complexes. J. Appl. Polym. Sci. 107 (4), 2280–2288.
Ahamad, T., Ruksana, Chaudhary, A.A., Naushad, M., Alshehri, S.M., 2019e. Fabrication of MnFe2O4 nanoparticles embedded chitosan-diphenylureaformaldehyde resin for the removal of tetracycline from aqueous solution. Int. J. Biol. Macromol. 134, 180–188.
Al-Enizi, A.M., Naushad, M., Al-Muhtaseb, A.A.H., Ruksana, Alshehri, S.M., Alothman, Z.A., Ahamad, T., 2018. Synthesis and characterization of highly selective and sensitive Sn/SnO2/N-doped carbon nanocomposite (Sn/SnO2@NGC) for sensing toxic NH3 gas. Chem. Eng. J. 345, 58–66.
Al-Farraj, E.S., Alhabarah, A.N., Ahmad, J., Al-Enizi, A.M., Naushad, M., Ubaidullah, M., Alshehri, S.M., Ruksana, Ahamad, T., 2018. Fabrication of hybrid nanocomposite derived from chitosan as efficient electrode materials for supercapacitor. Int. J. Biol. Macromol. 120, 2271–2278.
Al-Kahtani, A.A., Almuqati, T., Alhokbany, N., Ahamad, T., Naushad, M., Alshehri, S. M., 2018. A clean approach for the reduction of hazardous 4-nitrophenol using gold nanoparticles decorated multiwalled carbon nanotubes. J. Cleaner Prod. 191, 429–435.
Al-Kahtani, A.A., Alshehri, S.M., Naushad, M., Ruksana, Ahamad, T., 2019. Fabrication of highly porous N/S doped carbon embedded with ZnS as highly efficient photocatalyst for degradation of bisphenol. Int. J. Biol. Macromol. 121, 415–423.
Alhokbany, N., Ahama, T., Ruksana, Naushad, M., Alshehri, S.M., 2019. AgNPs embedded N- doped highly porous carbon derived from chitosan based hydrogel as catalysts for the reduction of 4-nitrophenol. Compos. Part B: Eng. 173, 106950.
Alshehri, S.M., Ahamad, T., 2013. Thermal degradation and evolved gas analysis of N, N '-bis(2 hydroxyethyl) linseed amide (BHLA) during pyrolysis and combustion. J. Therm. Anal. Calorim. 114 (3), 1029–1037.
Alshehri, S.M., Al-Fawaz, A., Ahamad, T., 2013. Thermal kinetic parameters and evolved gas analysis (TG-FTIR-MS) for thiourea-formaldehyde based polymer metal complexes. J. Anal. Appl. Pyrol. 101, 215–221.
Alshehri, S.M., Aldalbahi, A., Al-Hajji, A.B., Chaudhary, A.A., Panhuis, M., Alhokbany, N., Ahamad, T., 2016. Development of carboxymethyl cellulose-based hydrogel and nanosilver composite as antimicrobial agents for UTI pathogens. Carbohydr. Polym. 138, 229–236.
Alshehri, S.M., Alhabarah, A.N., Ahmed, J., Naushad, M., Ahamad, T., 2018. An efficient and cost-effective tri-functional electrocatalyst based on cobalt ferrite embedded nitrogen doped carbon. J. Colloid Interface Sci. 514, 1–9.
Choi, Y.-K., Kan, E., 2019. Effects of pyrolysis temperature on the physicochemical properties of alfalfa-derived biochar for the adsorption of bisphenol A and sulfamethoxazole in water. Chemosphere 218, 741–748.
Guo, Y., He, J., Wang, T., Xue, H., Hu, Y., Li, G., Tang, J., Sun, X., 2011. Enhanced electrocatalytic activity of platinum supported on nitrogen modified ordered mesoporous carbon. J. Power Sources 196 (22), 9299–9307.
Kurmus, H., Mohajerani, A., 2020. The toxicity and valorization options of cigarette butts. Waste Manage. 104, 104–118.
Liu, J., Jiang, S., Chen, D., Dai, G., Wei, D., Shu, Y., 2020. Activation of persulfate with biochar for degradation of bisphenol A in soil. Chem. Eng. J. 381, 122637.
Liu, N.-L., Dutta, S., Salunkhe, R.R., Ahamad, T., Alshehri, S.M., Yamauchi, Y., Hou, C.-H., Wu, K.C.-W., 2016. ZIF-8 derived, nitrogen-doped porous electrodes of carbon polyhedron particles for high-performance electrosorption of salt ions. Sci. Rep. 6 (1), 1–7.
Naushad, M., Ahamad, T., Al-Maswari, B.M., Abdullah Alqadami, A., Alshehri, S.M., 2017. Nickel ferrite bearing nitrogen-doped mesoporous carbon as efficient adsorbent for the removal of highly toxic metal ion from aqueous medium. Chem. Eng. J. 330, 1351–1360.
Nishat, N., Hasnain, S., Ahmad, T., Parveen, A., 2011. Synthesis, characterization, and biological evaluation of new polyester containing Schiff base metal complexes. J. Therm. Anal. Calorim. 105 (3), 969–979.
Park, C.M., Wang, D., Han, J., Heo, J., Su, C., 2019. Evaluation of the colloidal stability and adsorption performance of reduced graphene oxide–elemental silver/magnetite nanohybrids for selected toxic heavy metals in aqueous solutions. Appl. Surf. Sci. 471, 8–17.
Rong, X., Xie, M., Kong, L., Natarajan, V., Ma, L., Zhan, J., 2019. The magnetic biochar derived from banana peels as a persulfate activator for organic contaminants degradation. Chem. Eng. J. 372, 294–303.
Shokry, H., Elkady, M., Hamad, H., 2019. Nano activated carbon from industrial mine coal as adsorbents for removal of dye from simulated textile wastewater: operational parameters and mechanism study. J. Mater. Res. Technol. 8 (5), 4477–4488.
Soliman, N.K., Moustafa, A.F., Aboud, A.A., Halim, K.S.A., 2019. Effective utilization of Moringa seeds waste as a new green environmental adsorbent for removal of industrial toxic dyes. J. Mater. Res. Technol. 8 (2), 1798–1808.
Sophia, A., Lima, E.C., 2018. Removal of emerging contaminants from the environment by adsorption. Ecotoxicology and Environ. Saf. 150, 1–17.

Wang, B., Zeng, D., Chen, Y., Belzile, N., Bai, Y., Zhu, J., Shu, J., Chen, S., 2019a. Adsorption behaviors of phenanthrene and bisphenol A in purple paddy soils amended with straw-derived DOM in the West Sichuan Plain of China. Ecotoxicol. Environ. Saf. 169, 737–746.

Wang, L., Zhou, L., Fan, D., Wang, Z., Gu, W., Shi, L., Liu, J., Yang, J., 2019b. Bisphenol P activates hormonal genes and introduces developmental outcomes in Chironomus tentans. Ecotoxicol. Environ. Saf. 174, 675–682.

Wen, X., Lu, X., Xiang, K., Xiao, L., Liao, H., Chen, W., Zhou, W., Chen, H., 2019. Nitrogen/sulfur co-doped ordered carbon nanoarrays for superior sulfur hosts in lithium-sulfur batteries. J. Colloid Interface Sci. 554, 711–721.

Xiao, M., Meng, Y., Li, Y., Liu, X., Ke, X., Ren, G., Zhu, F., 2019. Tailoring nitrogen content in doped carbon by a facile synthesis with ionic liquid precursors for lithium ion batteries. Appl. Surf. Sci. 494, 532–539.

Xiaoying, M., Guangming, Z., Chang, Z., Zisong, W., Jian, Y., Jianbing, L., Guohe, H., Hongliang, L., 2009. Characteristics of BPA removal from water by PACl-Al13 in coagulation process. J. Colloid Interface Sci. 337 (2), 408–413.

Yu, C., Hou, H., Liu, X., Han, L., Yao, Y., Dai, Z., Li, D., 2018. The Recovery of the Waste Cigarette Butts for N-Doped Carbon Anode in Lithium Ion Battery. Front. Mater. 5 (63).

Zhang, J., Wang, Z., Fan, M., Tong, P., Sun, J., Dong, S., Sun, J., 2019. Ultra-light and compressible 3D BiOCl/ RGO aerogel with enriched synergistic effect of adsorption and photocatalytic degradation of oxytetracycline. J. Mater. Res. Technol. 8 (5), 4577–4587.